Gold on Carbon Catalyzed Conversion of Quadricyclane to Norbornadiene

ChemCatChem

ChemCatChem
Chemistry Europe
European Chemical Societies Publishing

RESEARCH ARTICLE OPEN ACCESS

Gold on Carbon Catalyzed Conversion of Quadricyclane to Norbornadiene

Zhihang Wang[1] | Lucien Magson[2] | Lorette Fernandez[3] | Helen Hölzel[3,4] | Pedro Ferreira[3] | Ignacio Funes-Ardoiz[2] | Robson Rosa da Silva[5] | Diego Sampedro[2] | Kasper Moth-Poulsen[3,5,6,7]

[1]School of Engineering, College of Science and Engineering, University of Derby, Derby, UK | [2]Departamento De Química, Instituto De Investigación Química De La Universidad de La Rioja (IQUR), Universidad De La Rioja, La Rioja, Spain | [3]Department of Chemical Engineering, Universitat Politècnica de Catalunya, Barcelona, Spain | [4]Institute of Organic Chemistry, Justus-Liebig-University Giessen, Giessen, Germany | [5]Department of Chemistry and Chemical Engineering, Chalmers University of Technology, Gothenburg, Sweden | [6]The Institute of Materials Science of Barcelona, Barcelona, Spain | [7]Catalan Institution for Research & Advanced Studies, Barcelona, Spain

Correspondence: Kasper Moth-Poulsen (kasper.moth-poulsen@upc.edu)

Received: 26 December 2025 | **Revised:** 13 May 2026 | **Accepted:** 5 June 2026

Keywords: catalyst | catalytic mechanism | density functional theory | molecular solar thermal (MOST) energy storage | photoswitch

ABSTRACT

The norbornadiene (NBD)–quadricyclane (QC) photoswitch system has emerged as a promising candidate for molecular solar thermal (MOST) energy storage, enabling solar energy capture and on-demand heat release. A critical step in these systems is the catalytic back-conversion of QC to NBD, which governs energy release efficiency. While noble metal catalysts have previously demonstrated activity, their long-term stability and scalability remain major challenges. In this study, we introduce a heterogeneous catalyst composed of 2–3 nm gold nanoparticles supported on Vulcan carbon (Au@Vulcan) for QC to NBD conversion. Three different QC derivatives with distinct substitution motifs displayed efficient back-conversion, as confirmed by NMR and UV–vis spectroscopy. Mechanistic insights into the QC to NBD isomerization, obtained from density functional theory (DFT) calculations on a model gold trimer, revealed two viable pathways: a concerted mechanism and a single-electron transfer mediated route. ICP-MS stability tests indicated partial gold leaching, underscoring the need for improved anchoring strategies to enhance catalyst durability under specified reaction conditions. Together, these findings demonstrate both the catalytic potential and limitations of Au@Vulcan, providing a framework for the rational design of more durable, cost-effective MOST catalysts and guiding future development of NBD derivatives towards a fast, responsive energy release process.

1 | Introduction

Due to the increasing challenges with fossil fuels driven by a growing population, harnessing solar energy in different forms is emerging as one of the most promising solutions [1, 2]. It has been estimated that seven hours of sunlight could fulfil the world's energy demand for an entire year [3]. Various solar technologies are being explored, including photovoltaics [4, 5], solar-driven water splitting [6, 7], solar water heating [8, 9], and applications in building design [10]. Among these, the use of photoswitchable molecules to store solar energy, known as molecular solar thermal (MOST) energy storage has garnered significant attention [11, 12]. The MOST system leverages photoswitchable molecules that absorb sunlight and undergo photoisomerization to a metastable high-energy state. Ideally, this photoisomer can be kept for extended periods of time. When the stored energy is needed, an

Zhihang Wang and Lucien Magson contributed equally to this work.

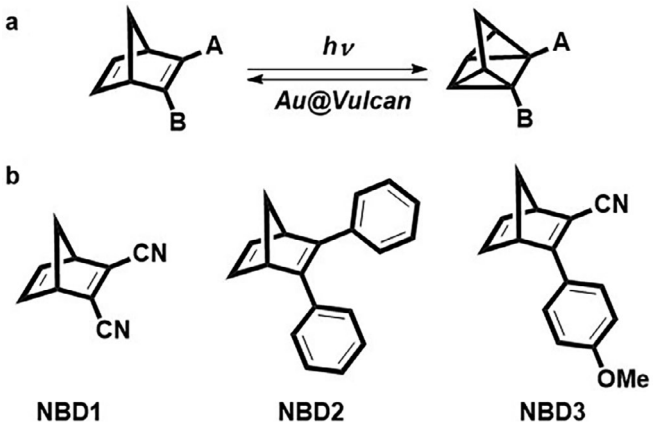

FIGURE 1 | (a) Schematic of the conversion and back-conversion of NBD–QC, where A and B denote different substituent groups. (b) Molecular structures of **NBD1–3** studied in this work. For the conversion reactions, **NBD1** was irradiated at 300 nm, while **NBD2** and **NBD3** were irradiated at 340 nm. All back-conversion reactions with the Au@Vulcan catalyst were carried out at room temperature.

efficient triggering agent, such as a catalyst, can be applied to release it as heat on demand, while converting the photoisomer back to its parent state [13]. In this context, extensive efforts have been devoted to tailoring the norbornadiene-quadricyclane pair (NBD-QC) (Figure 1a) [13–15], to enhance their molecular charging parameters, including solar spectral absorption [16, 17], thermal storage half-life [18], and energy storage density [19]. However, the catalytic back conversion process has received much less attention compared to the energy storage process. Libuda et al. investigated metallic Pt as an efficient catalyst for QC back conversion [20]. However, Pt can degrade the photoisomer via coke formation as it is also an efficient dehydrogenation catalyst. Subsequently, gold surfaces were explored [21–23]. Yet, gold is an expensive metal, making it impractical for large-scale applications if required in large amounts. Thus, minimizing the amount of gold, such as using gold nanoparticles, presents a way to reduce the overall amount used. In the search for alternatives, a protocol for the comparison of different heterogeneous catalysts was developed [24, 25]. In a batch examination, a series of heterogeneous catalysts were studied, identifying a Cu/C non-noble metal catalyst exhibiting comparable efficiency to a Pt/C catalyst [26, 27]. Complementary simulations of reactions in flow determined the catalyst particle size as crucial in achieving high yields, and reducing the total metal content is essential to increasing heat release [20].

The aim of this study is to elucidate why colloidal gold nanoparticles supported on carbon (Au@Vulcan) display pronounced catalytic activity in the isomerization of quadricyclane (QC) to norbornadiene (NBD). To uncover potential structure–property relationships, the catalytic back-reactions of three QC derivatives were investigated by NMR spectroscopy, with kinetic parameters quantified using UV–vis spectroscopy. These experimental insights were complemented by density functional theory (DFT) calculations in which an Au_3 cluster was used to represent the active site. This has enabled the construction of a detailed reaction mechanism and provided molecular-level understanding of how Au@Vulcan operates as a model heterogeneous catalyst for this isomerization.

2 | Results and Discussion

The commercially available catalyst comprises nanoscale colloidal gold nanoparticles impregnated onto a Vulcan XC72R carbon black support (see Supporting Information Section 2). Detailed characterization was undertaken because the physicochemical properties of Au@Vulcan can vary between batches, and such variations are critical for accurate mechanistic interpretation. Catalytic performance is strongly influenced by particle size, morphology, crystallinity, dispersion, and metal–support interactions, all of which must be carefully defined to enable meaningful comparison with DFT-supported reaction pathways. Advanced characterization techniques, including transmission electron microscopy (TEM), X-ray photoelectron spectroscopy, X-ray diffraction, and thermal analysis, were employed to validate the particle size, morphology, and composition. TEM images reveal predominantly spherical nanoparticles with internal contrast variations, consistent with a polycrystalline nature. Most nanoparticles are well-dispersed across the carbon support, indicating relatively uniform distribution and consistency across samples. Particle size distribution analysis confirms a narrow size range centered at 2–3 nm, with no particles exceeding 5 nm among approximately 200 measured (Figure 2b, see Supporting Information, Section 1, Table S1). Nonetheless, TEM micrographs occasionally show larger features exceeding 5 nm in size. The low frequency of such aggregates underscores the overall uniformity of the catalyst and supports its suitability for analytical catalytic batch testing. The X-ray photoelectron spectroscopy (XPS) spectrum exhibited characteristic Au 4f spin–orbit splitting peaks at binding energies of 84.0 eV (Au $4f_{7/2}$) and 88.0 eV (Au $4f_{5/2}$), which are characteristic of metallic gold (Au^0) (see Supporting Information Section 1, Figures S1 and S2). X-ray diffraction (XRD) analysis reveals a diffraction pattern consistent with the *Fm-3m* space group, characteristic of the face-centred cubic structure of gold nanoparticles, with reflections indexed to (111), (200), (220), (311), and (222) (see Supporting Information Section 1, Figure S3, Table S2). The pronounced peak intensities indicate high crystallinity, while slight broadening reflects the presence of multiple crystalline domains. In contrast, the weak, broad feature at ~26° arises from the amorphous carbon (002) reflection of the Vulcan support. The mean crystallite size, calculated using the Debye–Scherrer equation from the principal (111) diffraction peak at ~38.5°, was determined to be 8.6 nm, in comparison with TEM, further corroborating the polycrystalline character of the nanoparticles. Importantly, the diffraction pattern shows no additional reflections attributable to gold oxides or other crystalline phases [28]. Thermogravimetric analysis (TGA) was conducted on the Au@Vulcan composite, in which the onset of decomposition occurs at approximately 240°C. Taking the first derivative of the TGA curve from the initial plateau, a gold content of 35.1% was determined. Finally, two weight loss steps occur, indicated by the varying slopes, signifying the decomposition of two species, the first shallower slope likely being attributed to the loss of water molecules and the second, much steeper one, ascribed to a phase change in the material (see Supporting Information Section 1, Figure S4). For the study of catalytic QC to NBD conversion, three NBD derivatives were selected (Figure 1b). **NBD1** and **NBD2** are symmetrical NBDs with simple structures. **NBD1** features two electron-withdrawing groups [29], while **NBD2**, as previously reported [16], exhibits a redshift in the absorption spectrum due to the presence of two diphenyl groups.

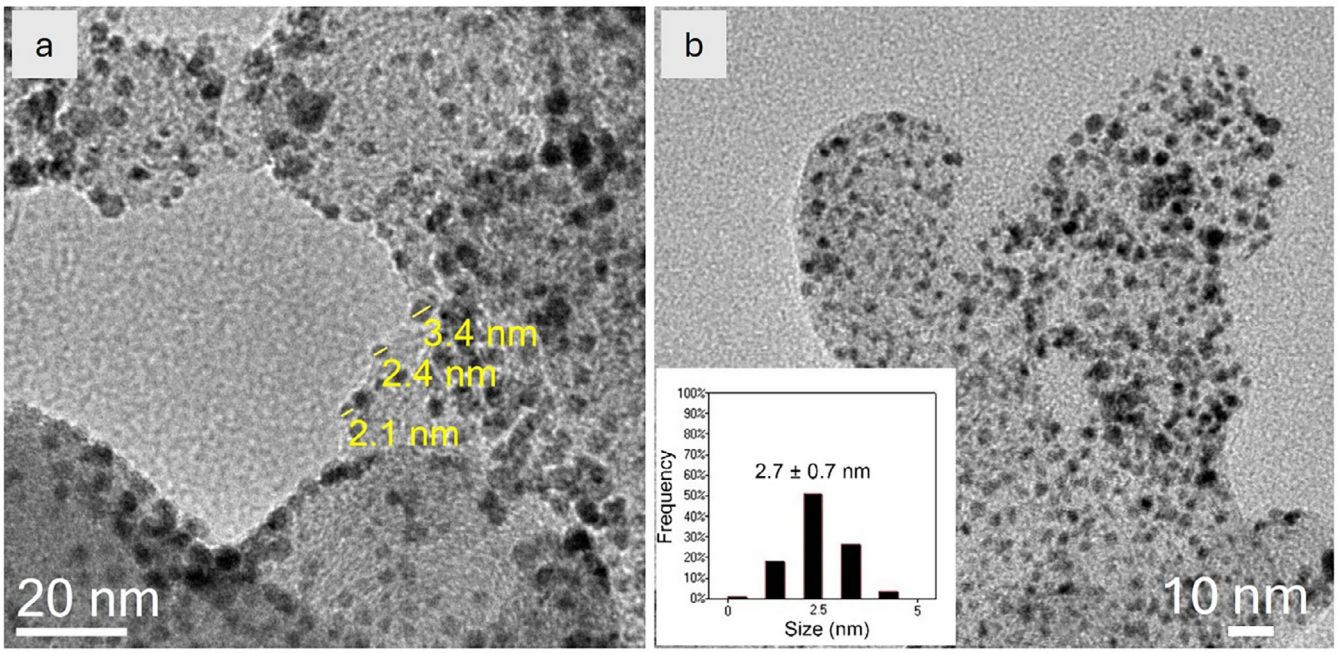

FIGURE 2 | (a) TEM image of Au@Vulcan. (b) TEM image with higher magnification. The inset shows the histogram of particle size distribution. Measurements were performed on 200 nanoparticles using the software Nano Measurer (version 1.2.5) developed by Jie Xu, Department of Chemistry, Fudan University, China.

The more polar **NBD3** contains a donor-acceptor motif designed to enhance solar light absorption [19]. The **NBD2** and **NBD3** derivatives have promising energy storage densities of up to 109 kJ mol^{-1} and 89 kJ mol^{-1} and storage lifetimes of approximately 43 and 30 days, respectively. To confirm the Au@Vulcan catalytic activity and selectivity, the catalytic reactions were monitored using ^{1}H NMR (see Supporting Information Section 3, Figure S5 and S6).

Nuclear magnetic resonance (NMR) analysis confirmed that all three QC photoisomers were converted to their corresponding NBD isomers, with no detectable side products (Figure 3; see also Figures S3 and S4 for **NBD1** and **NBD2**). Although the reactions proceeded with high selectivity, the post-reaction spectra of **NBD1** and **NBD3** showed reduced signal intensity relative to the starting materials, indicating incomplete conversion. Given the quantitative uncertainty of ±10% inherent to NMR integration, the reaction rates of **QC2** and **QC3** were further examined by UV–vis spectroscopy. Using the Beer–Lambert law, the starting and final concentrations of the respective NBD products were determined, providing a more reliable measure of conversion efficiency. In contrast, the back-conversion of **QC1** could not be reliably assessed because **NBD1** formation occurs near the cutoff wavelength of toluene, while the minimal blue-shift of **QC1** prevents selective UV–vis monitoring of product formation. Kinetic studies (see Supporting Information Section 4, Table S3) revealed that both **QC2** and **QC3** undergo catalytic back-conversion via a two-step process, comprising an initial kinetically active regime followed by a transport-mediated phase (see Supporting Information Section 4, Figure S7, Table S4). For **NBD2**, the initial rate decelerates after 15 min of reaction, and after 30 min for **NBD3**, with a significant difference in preliminary rates, changing from 10^{-2} (s^{-1}) for **QC3** to 10^{-3} (s^{-1}) for **QC2**. From that point onwards, both reactions proceed at a similar rate (10^{-3} s^{-1}). The overall conversion observed for both reactions after 2 h was 29 % and 97 %, respectively. To assess the stability of the Au@Vulcan catalyst, inductively coupled plasma mass spectrometry (ICP-MS) was performed using **QC3** (see Supporting Information section 4, Tables S5 and S6). The analysis revealed that an oxidative-induced gold leaching occurs during the back-conversion process, indicating that high-energy surface sites on the carbon support are prone to instability. This observation suggests that future catalyst design may benefit from surface modifications or anchoring strategies to enhance nanoparticle retention. The pronounced initial activity of Au@Vulcan is therefore attributed to the intrinsic reactivity of the supported nanoparticles, whereas sustained reactivity may arise from gold species becoming dispersed into solution. Guided by these findings, and as the central focus of this work, the catalytic mechanisms of **QC2** and **QC3** were subsequently investigated through computational studies. Focusing on the mechanism of the catalysed reaction, the free energy profile of the reaction mechanism was computed at the SMD (toluene) M06/Def2TZVPP//M06L/Def2SVP level of theory, employing a simplified Au_3 cluster model for the nanoparticle. This approach has been successfully used for nanoparticle and nanocluster simulations in related studies [30, 31]. (Figure 3, see Supporting Information section 5 for detailed computational results). The Au_3 cluster is considered a good representation of the active site in Au/C catalyst, because on the Au(111) surface, higher catalytic turnover is likely to occur at low-coordination sites such as edges, corners or small clusters.

The reaction starts with a weak coordination of the Au_3 core to the **QC3** substrate. Depending on whether activation occurs at the CN side or the aryl side, three distinct reaction pathways were identified, all leading exergonically to **NBD3**, with a total energy release of 20.4 kcal mol^{-1}. First, the activation of the C—C bond

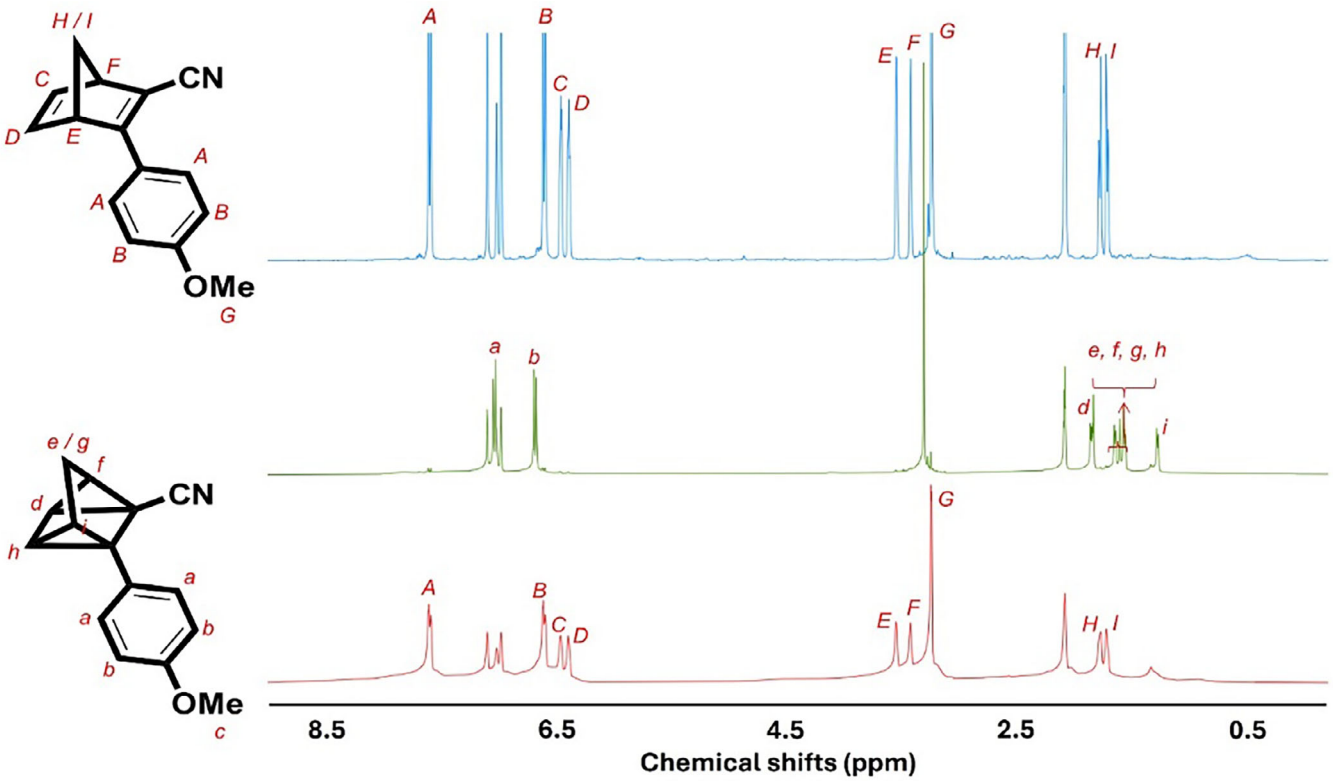

FIGURE 3 | NMR catalyst tests for **NBD3** (signals designated with upper case letters). The blue spectrum represents the initial **NBD3** molecules before irradiation. The green spectrum shows the **QC3** molecules (signals designated with lower case letters) after overnight irradiation with an LED light source (340 nm). The red spectrum was recorded after 1 h of Au@Vulcan catalyst addition (signals attributed are of **NBD3**).

near the CN group (highlighted in blue, CN side initiation) was analysed. Although the non-covalent coordination of the gold nanocluster on the CN side yields the more thermodynamically stable product, the rate determining transition state $\mathbf{Au_3\text{-}TS_{SET1}}$ (blue) is the highest found among the different reaction pathways (23.1 kcal mol^{-1}). Along the reaction coordinate, a formal electron transfer from the gold nanocluster to the QC enables the C—C bond breaking, generating a radical character in the C atom adjacent to the CN group. This step is exergonic by 10.7 kcal mol^{-1} and irreversible. Then, the second C—C bond breaking occurs via a radical reorganization step through a barrier of 9.6 kcal mol^{-1}. Finally, Au-C bond breaking allows the generation of the second NBD double bond and the back single electron transfer from the substrate to the Au_3 nanocluster, through a very small barrier of 3.6 kcal mol^{-1}. Although the overall process is redox neutral, the redox-active nature of the Au(0) nanocluster enables a previously unreported mechanism for QC-to-NBD conversion. The alternative initiation side, with coordination of Au_3 nanocluster next to the aryl group, was also explored (red pathway on Figure 4). Despite the weaker coordination in this side (−8.5 kcal mol^{-1} vs. −10.3 kcal mol^{-1} at the CN side), the related free energy profile has a more accessible free energy barrier. After the electron transfer from Au_3 to the QC substrate, the radical generated next to the aryl group produces a more stable intermediate, which can be efficiently delocalized in $^{s}\mathbf{Au_3}\text{-}^{d}\mathbf{INT_{SET1}}$ intermediate. The higher exergonicity of this step implies a reduction of the free energy barrier by 2.5 kcal mol^{-1}. In addition, we identified a concerted C–C bond-breaking step (black pathway) in which two Au–C bonds are formed. This step formally oxidizes the Au_3 nanocluster by two electrons and generates spin densities of 0.08, 0.33, and 0.59 electrons on the three gold centres. The efficient charge and spin delocalization along the gold nanocluster and the relatively strong character of the Au-C bond interaction make this pathway the most favoured one, through a free energy barrier of 14.2 kcal mol^{-1}. This low energy span matches the fast turnover of the gold catalyst. Subsequently, the $^{s}\mathbf{Au_3}\text{-}^{d}\mathbf{INT_{C1}}$ intermediate rapidly evolves into the more stable $^{s}\mathbf{Au_3}\text{-}^{d}\mathbf{INT_{SET1}}$ species through Au–C bond cleavage and formal oxidation of the Au_3 nanocluster. This transformation occurs via a barrierless process, with a calculated potential energy barrier of 0.5 kcal mol^{-1}, which becomes negative after free energy correction, indicating a spontaneous, energetically downhill pathway. From this point, the second C—C bond breaking and radical reorganization step is now endergonic, through a barrier of 11.3 kcal mol^{-1} free energy barrier. Finally, the unstable intermediate $^{s}\mathbf{Au_3}\text{-}^{d}\mathbf{INT_{SET2}}$ is further reduced by the Au_3 nanocluster, forming the final NBD product exergonically through a low barrier of 7.2 kcal mol^{-1}.

Results shown in Figure 4 are in good agreement with the experimental results. For the three computed paths, energy barriers show a preference for the concerted pathway, as they feature smaller free energy barriers. This aligns with the experimentally observed reaction behaviour. After calculating the same profile for **NBD2** (see Supporting Information Section 5, Figure S9), we found that the free energy barriers for each step in both pathways are lower for the QC3 derivative, leading to faster back-conversion kinetics. slightly higher barriers in the rate-determining steps for both concerted and SET (single-electron

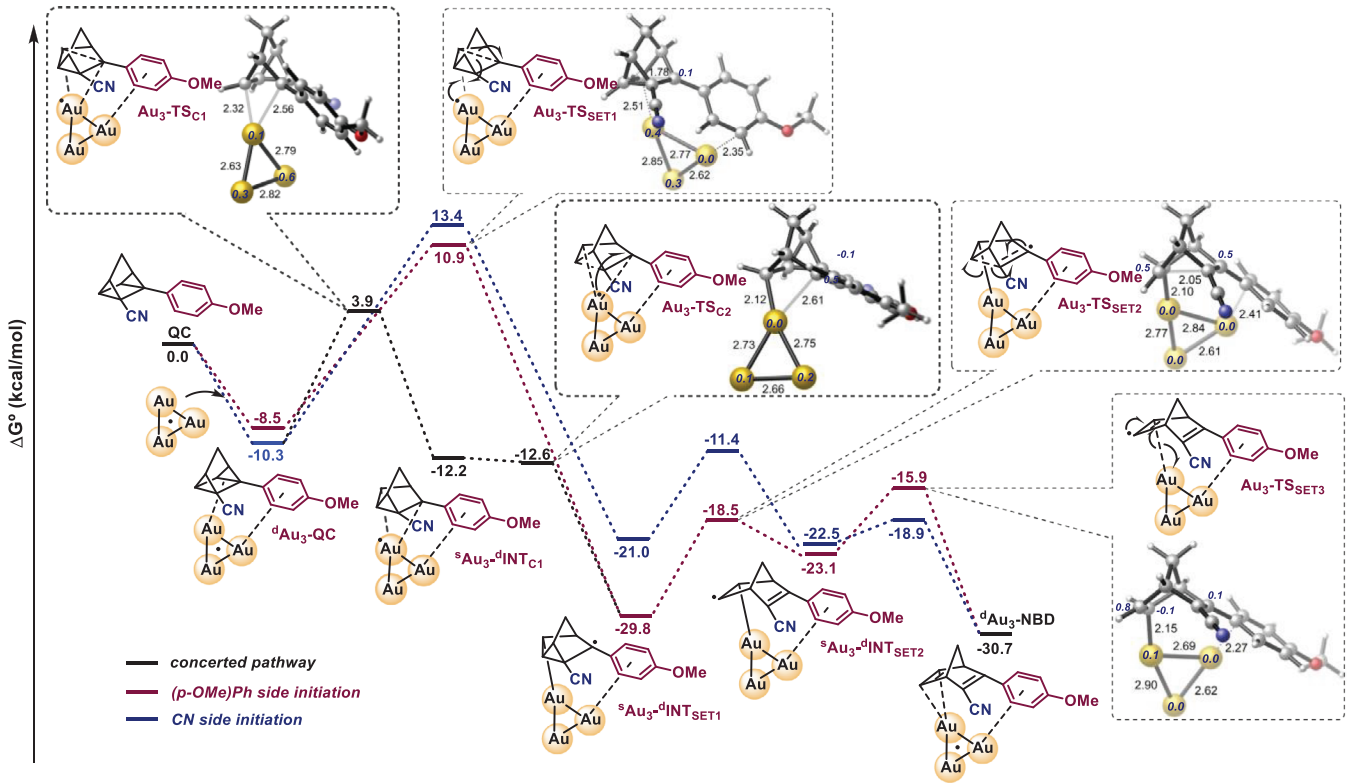

FIGURE 4 | Free energy profile of the different reaction pathways at SMD (toluene) M06/Def2TZVPP//M06L/Def2SVP level of theory. Energies in kcal mol^{-1}, bond distances in Å, and spin densities in a.u. (blue) are shown.

transfer) pathways compared to **NBD3**. This is consistent with the slower kinetic rate evolution of **QC2** to **NBD2**. The presence of bulky bis-phenyl moieties prevents an optimal approach to the heterogeneous Au catalyst, restricting efficient approach towards the strained C—C bond. As the reaction progresses from **QC2** to **NBD2**, the bis-phenyl moieties adopt an increasingly planar conformation, which promotes stronger adsorption onto the Au@Vulcan catalyst. This enhanced adsorption enthalpy with the surface leads to product inhibition by limiting **NBD2** desorption into the reaction medium, thereby reducing experimental detectability of **NBD2**. Comparison of the alternative thermally activated back-conversion routes shows that **QC2** exhibits higher enthalpic and entropic barriers than **QC3**, reflected in its longer half-life. Overall, these findings indicate that the catalyst exerts a broadly similar influence on both isomers, while substitution motifs in NBD derivatives remain an important factor for future exploration of catalytic mechanisms and intrinsic performance.

3 | Conclusion

In conclusion, this study demonstrates the potential of Au@Vulcan as an efficient and scalable catalyst for the conversion of QC to NBD, as shown by NMR and kinetic UV–vis spectroscopic analysis and supported by DFT calculations. The catalytic mechanism, characterized by single-electron transfer and concerted pathways, highlights the unique redox properties of the Au@Vulcan system, which demonstrates high intrinsic reactivities towards QC to NBD isomerisation reactions. Compared with previously reported Pt-, Au-, and Co-based heterogeneous catalysts [12, 13, 19, 22, 23] for QC-to-NBD back-conversion, Au@Vulcan shows high intrinsic activity and good selectivity, although its long-term practical applicability is currently limited by partial gold leaching and the need for improved nanoparticle anchoring. These results further suggest that reducing nanoparticle loadings should enhance active site dispersion, maximize accessible surface area, and lower the overall gold requirement, thereby improving the cost-effectiveness and scalability of MOST systems for triggered heat release. An alternative strategy to improve activity, could be to modify the carbon support to augment the charge transfer behaviour as this can influence the electronic structure of Au. Future investigations, systematically evaluating catalyst stability over multiple cycles and identifying deactivation pathways, will be essential. Finally, preliminary evidence indicates that NBD substitution motifs influence back-conversion kinetics, highlighting the need to consider structural effects when designing new NBD derivatives for optimized MOST performance.

Acknowledgments

Zhihang Wang acknowledges financial support from the University of Derby through the Early Career Researcher (ECR) Development Fund 2025–26. Helen Hölzel acknowledges financial support from the Deutsche Forschungsgemeinschaft (DFG) Research Unit FOR5499 “Molekulares Management von Sonnenenergie—Chemie von MOST—Systemen” Project number 496207555 including project part D-Dev: Exploring MOST for/in devices. Funding from the EU (H2020-FETPROACT2019-951801; Molecular Solar Thermal Energy Storage Systems) and the European Research Council (ERC) under grant agreement CoG, PHOTHERM–

101002131, Göran Gustafsson Foundation, the Swedish Research Council, the Spanish Ministry for Science and Innovation (project LIPCES, PID2021-123873NB-I00) and the Catalan Institute of Advanced Studies (ICREA) is acknowledged. Diego Sampedro and Ignacio Funes-Ardoiz acknowledge TED2021-131896B–I00 and PID2024-161126NB-I00 funded by MCIN/AEI/10.13039/501100011033 / FEDER EU. Ignacio Funes-Ardoiz acknowledges MCIN/AEI/10.13039/501100011033 for the Ramón y Cajal (RYC2022-035776-I).

Conflicts of Interest

The authors declare the following competing financial interest(s): Kasper Moth-Poulsen and Robson Rosa da Silva are co-owners of NanoScientifica AB, and Robson Rosa da Silva serves as the company's CEO. NanoScientifica AB supplied the catalyst employed in the present study.

Data Availability Statement

The data that supports the findings of this study are available in the supplementary material of this article.

References

1. IEA, *World Energy Outlook* 2024.

2. N. S. Lewis and D. G. Nocera, "Powering the Planet: Chemical Challenges in Solar Energy Utilization," *Proceedings of the National Academy of Sciences* 103 (2006): 15729–15735, https://doi.org/10.1073/pnas.0603395103.

3. M. Perez and R. Perez, "Update 2022 – A Fundamental Look at Supply Side Energy Reserves for the Planet," *Solar Energy Advances* 2 (2022): 100014, https://doi.org/10.1016/j.seja.2022.100014.

4. M. Victoria, N. Haegel, I. M. Peters, et al., "Solar Photovoltaics is Ready to Power a Sustainable Future," *Joule* 5 (2021): 1041–1056, https://doi.org/10.1016/j.joule.2021.03.005.

5. M. Mani and R. Pillai, "Impact of Dust on Solar Photovoltaic (PV) Performance: Research Status, Challenges and Recommendations," *Renewable and Sustainable Energy Reviews* 14 (2010): 3124–3131, https://doi.org/10.1016/j.rser.2010.07.065.

6. X. Guan, S. Shen, and S. S. Mao, "Harvesting The Two-Electron Process for Solar Water Splitting," *Cell Reports Physical Science* 4 (2023): 101211.

7. R.-T. Gao, N. T. Nguyen, T. Nakajima, et al., "Dynamic Semiconductor-Electrolyte Interface for Sustainable Solar Water Splitting Over 600 h Under Neutral Conditions," *Science Advances* 9 (2023): eade4589, https://doi.org/10.1126/sciadv.ade4589.

8. R. Shukla, K. Sumathy, P. Erickson, and J. Gong, "Recent Advances in the Solar Water Heating Systems: A Review," *Renewable and Sustainable Energy Reviews* 19 (2013): 173–190, https://doi.org/10.1016/j.rser.2012.10.048.

9. N. V. Ogueke, E. E. Anyanwu, and O. V. Ekechukwu, "A Review of Solar Water Heating Systems," *Journal of Renewable and Sustainable Energy* 1 (2009): 043106.

10. J. Kanters and M. Horvat, "Solar Energy as a Design Parameter in Urban Planning," *Energy Procedia* 30 (2012): 1143–1152, https://doi.org/10.1016/j.egypro.2012.11.127.

11. K. Moth-Poulsen, D. Ćoso, K. Börjesson, et al., "Molecular Solar Thermal (MOST) Energy Storage and Release System," *Energy & Environmental Science* 5 (2012): 8534–8537, https://doi.org/10.1039/c2ee22426g.

12. Z. Yoshida, "New Molecular Energy Storage Systems," *Journal of Photochemistry* 29 (1985): 27–40, https://doi.org/10.1016/0047-2670(85)87059-3.

13. Z. Wang, P. Erhart, T. Li, et al., "Storing Energy With Molecular Photoisomers," *Joule* 5 (2021): 3116–3136, https://doi.org/10.1016/j.joule.2021.11.001.

14. J. Orrego-Hernández, H. Hölzel, Z. Wang, M. Quant, and K. Moth-Poulsen, "Norbornadiene/Quadricyclane (NBD/QC) and Conversion of Solar Energy," *Molecular Photoswitches* (Wiley, 2022), 351–378, https://doi.org/10.1002/9783527827626.

15. F. Hemauer, H.-P. Steinrück, and C. Papp, "The Norbornadiene/Quadricyclane pair as Molecular Solar Thermal Energy Storage System: Surface Science Investigations," *Chemphyschem* 25 (2024): e202300806.

16. V. Gray, A. Lennartson, P. Ratanalert, K. Börjesson, and K. Moth-Poulsen, "Diaryl-Substituted Norbornadienes With Red-Shifted Absorption for Molecular Solar Thermal Energy Storage," *Chemical Communications* 50 (2014): 5330–5332, https://doi.org/10.1039/C3CC47517D.

17. L. Fei, H. Hölzel, Z. Wang, et al., "Two-way Photoswitching Norbornadiene Derivatives for Solar Energy Storage," *Chemical Science* 15 (2024): 18179–18186, https://doi.org/10.1039/D4SC04247F.

18. M. Jevric, A. U. Petersen, M. Mansø, et al., "Norbornadiene-Based Photoswitches With Exceptional Combination of Solar Spectrum Match and Long-Term Energy Storage," *Chemistry—A European Journal* 24 (2018): 12767–12772, https://doi.org/10.1002/chem.201802932.

19. Z. Wang, A. Roffey, R. Losantos, et al., "Macroscopic Heat Release in a Molecular Solar Thermal Energy Storage System," *Energy & Environmental Science* 12 (2019): 187–193, https://doi.org/10.1039/C8EE01011K.

20. U. Bauer, S. Mohr, T. Döpper, et al., "Catalytically Triggered Energy Release From Strained Organic Molecules: The Surface Chemistry of Quadricyclane and Norbornadiene on Pt(111)," *Chemistry—A European Journal* 23 (2017): 1613–1622, https://doi.org/10.1002/chem.201604443.

21. R. Eschenbacher, F. Hemauer, E. Franz, et al., "Au-Catalyzed Energy Release in a Molecular Solar Thermal (MOST) System: A Combined Liquid-Phase and Surface Science Study," *ChemPhotoChem* 8 (2024): e202300155.

22. R. Eschenbacher, T. Xu, E. Franz, et al., "Triggering the Energy Release in Molecular Solar Thermal Systems: Norbornadiene-Functionalized Trioxatriangulen on Au(111)," *Nano Energy* 95 (2022): 107007, https://doi.org/10.1016/j.nanoen.2022.107007.

23. E. Franz, C. Stumm, F. Waidhas, et al., "Tunable Energy Release in a Reversible Molecular Solar Thermal System," *ACS Catalysis* 12 (2022): 13418–13425, https://doi.org/10.1021/acscatal.2c03043.

24. A. Giménez-Gómez, L. Magson, C. Merino-Robledillo, et al., "State-of-the-Art and Challenges Towards a Molecular Solar Thermal (MOST) Energy Storage Device," *Reaction Chemistry & Engineering* 9 (2024): 1629–1640.

25. A. Gimenez-Gomez, B. Rollins, A. Steele, et al., "Unveiling the Potential of Heterogeneous Catalysts for Molecular Solar Thermal Systems," *Chemistry–A European Journal* 30 (2024): e202303230.

26. L. Magson, H. Hölzel, A. S. Aslam, et al., "Synthesis and Characterization of Carbon-Based Heterogeneous Catalysts for Energy Release of Molecular Solar Thermal Energy Storage Materials," *ACS Applied Materials & Interfaces* 16 (2024): 7211–7218, https://doi.org/10.1021/acsami.3c16855.

27. L. Magson, D. Maggiolo, A. Sasic-Kalagasidis, et al., "Sustainable Heat Generation in Flow From a Molecular Solar Thermal Energy Storage System," *Advanced Energy and Sustainability Research* 6 (2025): 2400230, https://doi.org/10.1002/aesr.202400230.

28. S. Krishnamurthy, A. Esterle, N. C. Sharma, and S. V. Sahi, "Yucca-Derived Synthesis of Gold Nanomaterial and Their Catalytic Potential," *Nanoscale Research Letters* 9 (2014): 627, https://doi.org/10.1186/1556-276X-9-627.

29. M.-A. Martin-Drumel, J.-T. Spaniol, H. Hölzel, et al., "Searches for Bridged Bicyclic Molecules in Space—Norbornadiene and its Cyano Derivatives," *Faraday Discussions* 245 (2023): 284–297, https://doi.org/10.1039/D3FD00016H.

30. E. Fernández, M. A. Rivero-Crespo, I. Domínguez, et al., "Base-Controlled Heck, Suzuki, and Sonogashira Reactions Catalyzed by Ligand-Free Platinum or Palladium Single Atom and Sub-Nanometer

Clusters," *Journal of the American Chemical Society* 141 (2019): 1928–1940, https://doi.org/10.1021/jacs.8b07884.

31. J. Cordón, G. Jiménez-Osés, J. M. López-de-Luzuriaga, and M. Monge, "The Key Role of Au-substrate Interactions in Catalytic Gold Subnanocluster," *Nature Communications* 8 (2017): 1657.

Supporting Information

Additional supporting information can be found online in the Supporting Information section.

Supporting file: cctc70875-sup-0001-SuppMat.docx.